Geophys. J. Int. (2001) **144,** 206–220

Source parameters and tectonic origin of the 1996 June 1 Tianzhu ($M_w = 5.2$) and 1995 July 21 Yongden ($M_w = 5.6$) earthquakes near the Haiyuan fault (Gansu, China)

C. Lasserre,[1] B. Bukchin,[2] P. Bernard,[3] P. Tapponnier,[1] Y. Gaudemer,[1] A. Mostinsky[2] and Rong Dailu[4]

[1] *Laboratoire de Tectonique et Mécanique de la Lithosphère, CNRS UMR* 7578, *Institut de Physique du Globe de Paris, Paris, France. E-mail:lasserre@ipgp.jussieu.fr*
[2] *International Institute of Earthquake Prediction and Mathematical Geophysics, Moscow, Russia. E-mail: bukchin@mitp.ru*
[3] *Laboratoire de Sismologie, CNRS UMR* 7580, *Institut de Physique du Globe de Paris, Paris, France*
[4] *Seismological Institute of Lanzhou, China Seismological Bureau, Lanzhou, Gansu, China*

Accepted 2000 August 25. Received 2000 August 21; in original form 2000 February 22

SUMMARY

The 1996 June 1 Tianzhu ($M_w = 5.2$, $M_s = 4.9$) and the 1995 July 21 Yongden ($M_w = 5.6$, $M_s = 5.4$) earthquakes are the two largest events recorded in the last 10 years between the 1990 October 20 $M_s = 5.8$ and the recent 2000 June 6 $M_s = 5.6$ earthquakes near the 'Tianzhu seismic gap' on the Haiyuan fault in northeastern Tibet. We use frequency–time analysis (FTAN) to extract the fundamental modes of Love and Rayleigh waves from digital records. A joint inversion of their amplitude spectra and of *P*-wave first-motion polarities is then performed to calculate the source parameters (focal mechanisms, depths and seismic moments) of these two $M_s \simeq 5$ earthquakes. Such a joint inversion is tested for the first time. We use IRIS and GEOSCOPE network records for period ranges of 20–40 s for the former event and 35–70 s for the latter. The inversion of the Tianzhu earthquake yields nodal planes with strike, dip and slip of 282°, 72° and 3° and 191°, 87° and 162°, respectively, a focal depth around 12 km and a seismic moment of 0.56×10^{17} N m, consistent with the Harvard CMT calculation, and the alignment and depths of the aftershocks recorded by a local network. We propose two possible tectonic interpretations for this off-fault event. The solution for the Yongden earthquake is consistent with a thrust, with strike, dip and slip of 105°, 45° and 75°, respectively, a focal depth around 6 km and a seismic moment of 2.4×10^{17} N m, also in agreement with the Harvard CMT mechanism, the distribution of the aftershocks recorded by a regional network, and the general tectonic setting that we refine.

Key words: earthquake source mechanism, NE Tibet, *P* waves, seismic gap, seismotectonics, surface waves.

1 INTRODUCTION

The inversion of surface wave amplitude spectra, based on the method described by Bukchin (1989, 1990, 1995), has already demonstrated its reliability in the source mechanism determination of large earthquakes ($M_s \geq 6.5$). In particular, three major earthquakes of central Asia, the $M_s = 6.9$ 1988 Spitak event (Bukchin *et al.* 1994), the $M_s = 7.4$ 1992 Susamyr event (Gomez *et al.* 1997a) and the $M_s = 6.5$ 1992 Barisakho event (Gomez *et al.* 1997b), have been studied with this method, which proves to be a good complement to classical body wave modelling (Gomez 1998). To estimate the source parameters of relatively weak earthquakes ($M_w \simeq 5$), for which body wave inversion generally fails or reaches its limit, different methods using surface waves have recently been developed (e.g. Braunmiller *et al.* 1994; Arvidsson & Ekström 1998, and references therein). Until now, the inversion of surface wave amplitude spectra has never been used for source studies of such small events. Using surface wave amplitude spectra only, however, does not provide a unique focal mechanism solution (Mendiguren 1977). Additional information is needed to constrain the uniqueness of the solution; this was provided by long-period ($T \geq 100$ s) surface wave phase spectra in the aforementioned studies of large earthquakes and by *P*-wave first-motion polarities in this study. We test, for the first time, the feasibility of a joint inversion of surface wave amplitude spectra and *P*-wave first-motion polarities to calculate the source parameters of two moderate-sized earthquakes ($M_w \simeq 5.5$, $M_s \simeq 5$).

The two earthquakes we investigate are located in north-eastern Tibet: the Tianzhu earthquake (1996 June 1, $M_w = 5.2$, $M_s = 4.9$) and the Yongden earthquake (1995 July 21, $M_w = 5.6$, $M_s = 5.4$). Both of them occurred in regions adjacent to the $\simeq 1000$ km long Haiyuan fault system, the principal left-lateral strike-slip fault accommodating the eastward component of movement between Tibet and the Gobi-Ala Shan Platform due to India–Asia collision (Fig. 1; Tapponnier & Molnar 1977; Zhang *et al.* 1988a,b). In 1920 and 1927, this fault system experienced two $M \geq 8$ earthquakes, 300 km apart (Fig. 1; Deng *et al.* 1986; Zhang *et al.* 1987; Gaudemer *et al.* 1995). The Tianzhu and Yongden events took place near the 220 km long quiescent western segment of the Haiyuan fault—known as the 'Tianzhu seismic gap', a site of significant seismic hazard, $M \geq 7.5$ (Gaudemer *et al.* 1995; Lasserre *et al.* 1999)—between the 1920 and 1927 ruptures. A better understanding of their mechanism, in relation to the current deformation of the area, was thus required, which motivated this study. Between the 1990 October 20 $M_s = 5.8$ and the recent 2000 June 6 $M_s = 5.6$ earthquakes, both at the eastern end of the gap (Fig. 1), the Tianzhu and Yongden events are in fact the largest ones recorded near the gap. Furthermore, the Tianzhu earthquake is the largest event to occur less than 3 km from the Haiyuan fault trace, almost at the centre of the gap, since 1920. Its epicentre lies next to a 10 km wide pull-apart step between two segments of the fault (Tianzhu basin, Fig. 1) (Gaudemer *et al.* 1995), which could act as a nucleation zone for a future large earthquake in the gap (King & Nabelek 1985; Barka & Kadinsky-Cade 1988; Nielsen & Knopoff 1998). The Yongden event is further away from the Haiyuan fault but located less than 50 km northeast of Lanzhou, a city of three million people. The fault responsible for this earthquake was previously unknown.

We retrieved the Love and Rayleigh fundamental modes from the IRIS and GEOSCOPE broad-band digital records. A joint inversion of their amplitude spectrum and of *P*-wave first-motion polarities at worldwide stations or at Chinese regional stations was then performed to calculate the focal mechanism parameters (nodal plane strike, dip and slip angles), the depths and the seismic moments of the Tianzhu and Yongden events. The results are compared to available Harvard CMT solutions and, for the Tianzhu earthquake, to the Lanzhou Seismological Institute solution. The focal mechanisms of the Tianzhu and Yongden events are then discussed with regard to the distribution of their aftershocks, recorded by a local network and by the Chinese regional network, respectively, and interpreted in relation to the regional tectonics.

2 METHOD: JOINT INVERSION OF SURFACE WAVE AMPLITUDE SPECTRA AND *P*-WAVE FIRST-MOTION POLARITIES

We consider an instantaneous pure double-couple point seismic source of coordinate vector $\mathbf{y}$. The spectrum of displacements, $\mathbf{u}(\mathbf{x}, \omega)$, generated by such a source at an observation point $\mathbf{x}$ is related to the total moment tensor $\boldsymbol{M}$ by the eq.

$$u_n(\mathbf{x}, \omega) = \frac{1}{i\omega}\left(M_{kl}\,\frac{\partial}{\partial y_l}\,G_{nk}(\mathbf{x}, \mathbf{y}, \omega)\right), \tag{1}$$

where the summation convention for repeated subscripts is used, $n, k, l = 1, 2, 3$, and $G_{nk}(\mathbf{x}, \mathbf{y}, \omega)$ is the spectrum of the Green's function for a given wave type and medium (Levshin 1985; Bukchin 1990). In the case of a finite source, eq. (1) describes the spectrum of displacements for periods much longer than the source duration. The low-frequency displacement energy is mainly carried by surface waves. Only low-frequency displacements transported by the fundamental modes of the Love and Rayleigh waves will be considered here. We assume that variations of medium properties in any horizontal direction are small over distances along the wave paths of the order of a wavelength, so that the structure of the medium can be well approximated by a weak horizontally inhomogeneous model (Woodhouse 1974; Babich *et al.* 1976). The scattering of energy at subvertical boundaries is considered negligible; this has been verified for a large variety of models (Levshin 1985). Under these assumptions, the spectral parameters of the surface waves can be determined locally. The spectrum of the Green's function for Love and Rayleigh waves in eq. (1) depends on (1) the velocity and density models in the source region and under the seismic stations recording the earthquake, (2) the mean phase velocity of waves along the path between the source and the receiver and (3) geometrical spreading (Levshin 1985; Bukchin 1990). If all of these characteristics are known, as well as the origin time of the earthquake and the hypocentre location, recording $u_i(\mathbf{x}, \omega)$ at different points $\mathbf{x}$ on the Earth's surface for a set of frequencies ω gives, from eq. (1), a system of linear equations from which the elements of the seismic moment tensor M_{ij} can be retrieved. The mean phase velocity of surface waves, however, is usually poorly known. To calculate the source parameters, only the amplitude spectrum $|u(\mathbf{x}, \omega)|$, that is, the absolute value of the displacement spectrum $u(\mathbf{x}, \omega)$ described in eq. (1), is used, as its value does not depend on this average phase velocity. It is important to note also that the value of $|u(\mathbf{x}, \omega)|$ is not affected by any error in epicentre location (Bukchin 1990).

We assume now that the velocity and density of the propagating medium are given near the source and under each station at the free surface recording the seismic event and that all of the following hypotheses are valid: an instant point source on an ideal plane fault, with known origin time and epicentre location, and a medium with weak lateral inhomogeneities. The seismic source is then completely defined by its double-couple depth, its focal mechanism parameters—whether expressed by the strike, dip and slip angles of the nodal planes or by the two unit vectors $\mathbf{P}$ and $\mathbf{T}$ in the directions of principal compression and the tension axes, respectively—and its seismic moment M_0. To estimate these parameters, we construct a grid in the 4-D space of axis depth, strike, dip and slip, and for each point of this grid, using eq. (1), we calculate the amplitude spectra of the fundamental modes of both Love and Rayleigh waves at all the seismic stations used in the inversion for a set of frequencies ω (Levshin 1985; Bukchin 1990). A normalized residual of surface wave amplitude spectra $\varepsilon_{sw}(h, \mathbf{T}, \mathbf{P})$ is defined as

$$\varepsilon_{sw}(h, \mathbf{T}, \mathbf{P}) = \sqrt{\frac{\sum_{i=1}^{N} {\varepsilon_{sw}^{(i)}}^2}{\sum_{i=1}^{N} |u^{(i)}(\mathbf{x}, \omega)|^2_{obs}}}, \tag{2}$$

where h is the double-couple depth, N is the number of observations at seismic stations and

$$\varepsilon_{sw}^{(i)} = |u^{(i)}(\mathbf{x}, \omega)|_{obs} - |u^{(i)}(\mathbf{x}, \omega)|_{calc} \tag{3}$$

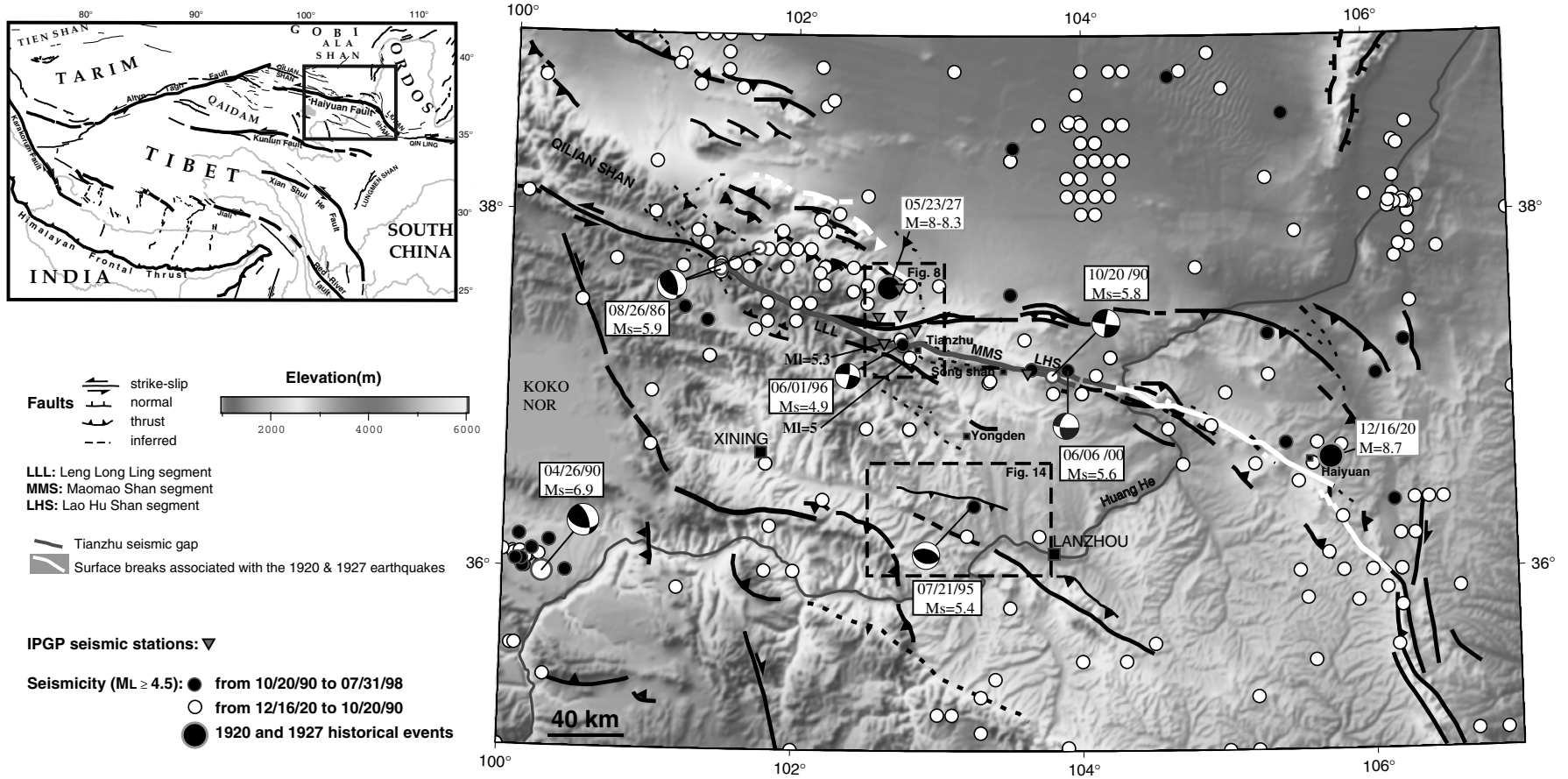

Figure 1. Seismotectonic map of the Haiyuan fault system (Gansu, China). Faults are from fieldwork or Landsat and SPOT image interpretation. The Tianzhu seismic gap is outlined in grey. Locations of 1920, 1927, 1986 and 1990 earthquakes are from Gaudemer *et al.* (1995). Location of 2000 event is from Seismological Institute of Lanzhou (SIL), focal mechanism from USGS. Other events are from Chen *et al.* (1991) (1920–1984), Center for analysis and Prediction, CSB (1989) (1984–1988) and SIL (1988–1998). White dots indicate events before the $M_s = 5.8$ 1990 event and black dots events after it. Topography is from 30 arc s Defense Mapping Agency DEM. Dashed black boxes show locations of Figs 8 and 14. Inset with box (top left) shows the tectonic setting of the Haiyuan fault within the India–Asia collision zone; the small black box shows the location of Fig. 1.

is the residual between the ith observed amplitude spectrum and the computed one. M_0 is calculated by minimizing the residual $\varepsilon_{sw}(h, \mathbf{T}, \mathbf{P})$ for each combination of all other parameters. If only absolute values of surface wave spectra are used, however, an ambiguity in source parameter determination remains and four equivalent solutions are obtained due to the sign ambiguity of moment tensor components and to the symmetry of the radiation patterns of surface wave amplitude spectra with respect to the epicentre (Mendiguren 1977). To resolve this ambiguity, we also use in the inversion the polarities of *P*-wave first motions at observation stations. For shallow sources (with a depth much smaller than the observed signal wavelength), the surface wave excitation by the vertical dip-slip component of the moment tensor is small. When calculating the moment tensor from surface wave analysis, this vertical dip-slip component is thus usually poorly resolved (Dziewonski *et al.* 1981; Given & Mellman 1986; Ekström & Richards 1994; Braunmiller *et al.* 1994). Using *P*-wave first-motion polarities as additional information in the inversion improves the resolution of this component and possibly of the source depth. A selection among available *P* polarities is made following the method described in Appendix A. For each focal mechanism, we calculate the theoretical radiation pattern of *P* waves and compare predicted and observed polarities. A residual ε_{pol} is defined as the ratio between the number of polarities inconsistent with the radiation pattern and the total number of observed polarities.

Eventually, for each possible combination of source parameters, we calculate a joint residual of surface wave amplitude spectra and *P*-wave first-motion polarities $\varepsilon(h, \mathbf{T}, \mathbf{P})$ defined by

$$\varepsilon(h, \mathbf{T}, \mathbf{P}) = 1 - (1 - \varepsilon_{pol})(1 - \varepsilon_{sw}) . \quad (4)$$

Minimizing $\varepsilon(h, \mathbf{T}, \mathbf{P})$ by a systematic exploration of the 4-D parameter space gives the best estimate of source parameters. To estimate the resolution of these parameters, we calculate partial residual functions. Fixing one of the parameters, h for instance, the combination of the other parameters that minimizes ε is searched for. This minimum value of ε is taken as the value of the partial residual function $\varepsilon_h(h)$, of scalar argument h, evaluated for each possible value of h. In the same way, partial residual functions of vectorial arguments $\mathbf{T}$ and $\mathbf{P}$, $\varepsilon_{\mathbf{T}}(\mathbf{T})$ and $\varepsilon_{\mathbf{P}}(\mathbf{P})$, are computed. The minimum of the partial residual functions corresponds to the best estimate of the associated parameter. These functions thus characterize the degree of resolution of each source parameter.

3 DATA ANALYSIS

For both the Tianzhu event and the Yongden event, the fundamental modes of Love and Rayleigh waves were retrieved from broad-band digital records of the IRIS and GEOSCOPE networks by frequency–time analysis (FTAN) and floating filtering of signals, as described by Lander 1989a and Levshin *et al.* (1994). An example of FTAN diagrams and seismograms is shown in Fig. 2. This type of analysis and filtering allows one to isolate the wave under study from the noise and to separate different waves. In the same filtering band, floating-filtered displacement amplitude spectra are smoother than classically filtered spectra and their inversion appears much more stable. The period range in which spectra of Love and Rayleigh wave fundamental modes were calculated depended on the event size. The instantaneous point source approximation considered to calculate surface wave amplitude spectra is valid only for periods much longer than the source duration. During FTAN, we thus selected, for each event, a period range in which surface waves were clearly isolated, covering the longest periods available. Signals showing polarization anomalies (analysed according to the method described by Lander 1989b) that were too large were rejected during the inversion process. The observed amplitude spectra at each station were corrected for attenuation during propagation and for instrumental response. Inversion of the source parameters of both earthquakes proceeded according to the hypotheses and technique described in Section 2.

3.1 Tianzhu earthquake

3.1.1 Results of inversion

A total of 11 IRIS and GEOSCOPE stations were selected for inversion. Their azimuthal distribution is shown in Fig. 3. Spectra of Love and Rayleigh fundamental modes, recorded at 10 and seven stations (Table 1), respectively, were used between periods of 20 and 40 s. The epicentre location (latitude: 37.283°, longitude: 102.75°) and the origin time (12:49:12.6 UT) of the earthquake chosen are those given by the Seismological Institute of Lanzhou (SIL), China Seismological Bureau, Gansu province. They were derived from records of the Gansu regional seismic network and are thus better constrained than those estimated by Harvard. In the source region, we used a regional velocity model, also from SIL, for the four upper layers and the PREM model below (Table 2). The crust in this SIL model is about 50 km thick, as expected in the shortening and thickening context of northeastern Tibet (Meyer *et al.* 1998), and is comparable to the 47.7 km thick crust under the Gobi desert (Ma 1987). Under the receivers, models were chosen among four classes: Gutenberg continental model, oceanic model and two 'tectonic' models with thickened crust (Tables 1 and 3) following previous studies (Gomez *et al.* 1997a,b). *P*-wave first-motion polarities at some stations of the Gansu seismic network complemented the set of polarities at worldwide stations. Our best estimate of the double-couple focal mechanism shows predominant strike-slip motion. The first nodal plane has a strike, dip and slip of 282°, 72° and 3°, respectively, and the

Table 1. Seismic stations, wave types and models used for the inversion of the Tianzhu earthquake.

Station	Wave type*	Model†
CHTO	L	1
HIA	R, L	1
MDJ	R, L	1
QIZ	R, L	1
SSE	R, L	1
LSA	R	2
ENH	R, L	3
KMI	R, L	3
TLY	L	3
ULN	L	3
WMQ	L	3

*R: Rayleigh; L: Love
†See Table 3

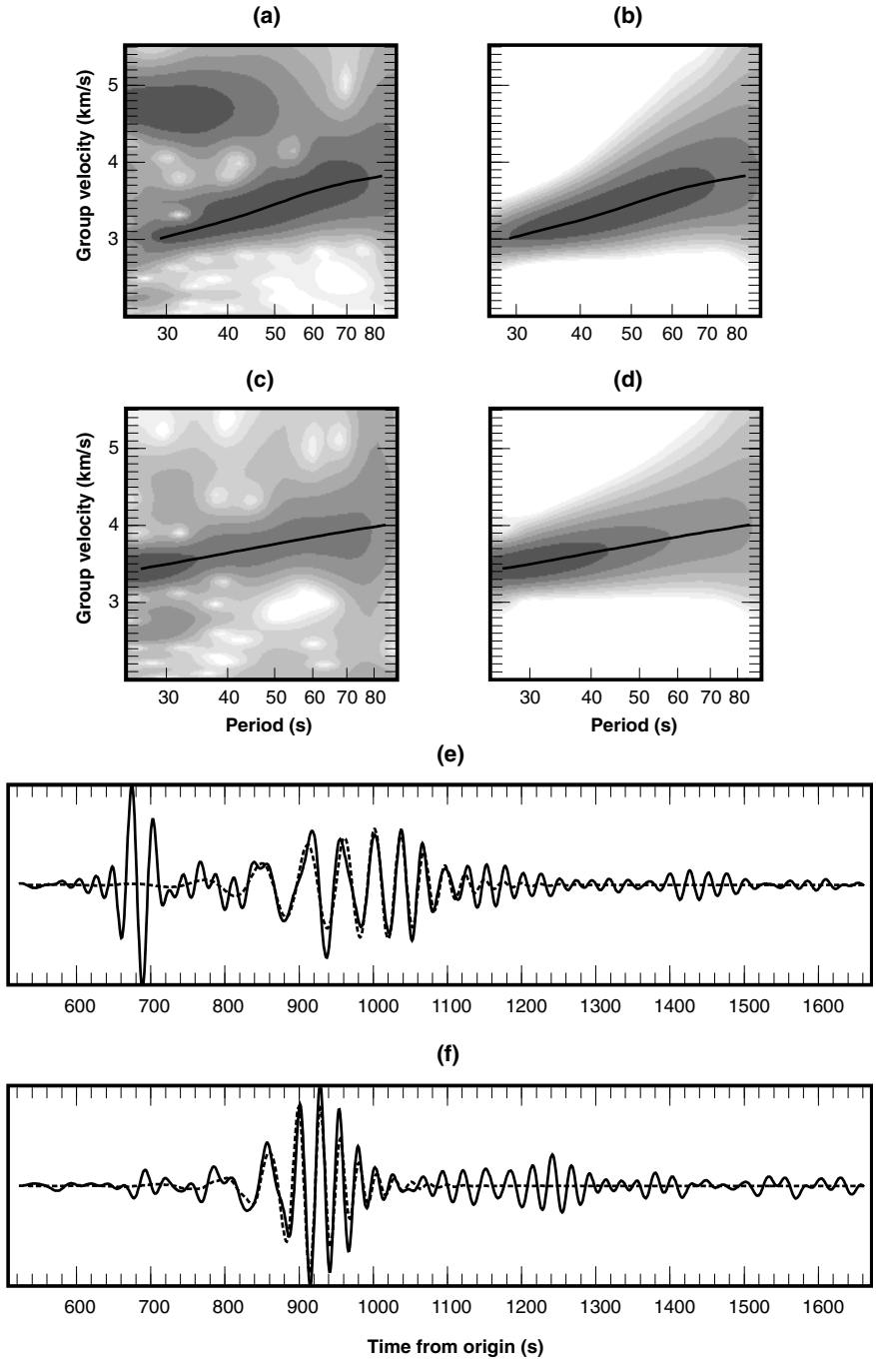

Figure 2. Example of FTAN analysis and floating filtering for the Yongden earthquake record at GEOSCOPE station HYB, isolating fundamental modes of Rayleigh and Love waves. FTAN diagrams for (a) raw and (b) floating-filtered vertical component, and for (c) raw and (d) floating-filtered transverse component. Solid line follows dispersion curve. (e) Vertical and (f) transverse components of raw record (solid line) and floating-filtered record (dashed line), normalized with respect to maximum observed amplitude.

Table 2. Source model.

Source model			
h (km)	V_P (km s^{-1})	V_S (km s^{-1})	ρ (g cm^{-3})
1.1	5.08	2.90	3.26
5.8	5.90	3.50	3.59
14.1	6.06	3.57	3.65
30.9	6.51	3.77	3.83

second, 191°, 87° and 162°, respectively (Figs 4a and b). This is in good agreement with the Harvard mechanism (Figs 4c and d). Available *P*-wave polarities in fact seem to match our focal mechanism better than the Harvard one (Figs 4b and d). For information, we present the SIL mechanism, computed from *P* polarities at Chinese regional stations (the detailed method of calculation is unknown): the strikes of the nodal planes compare well with ours but dips, particularly for the second nodal plane, differ significantly (Fig. 4e). The seismic moment we obtain is 0.56×10^{17} N m, somewhat smaller than

Table 3. Receiver models.

Model 1*				Model 2†				Model 3§				Model 4¶			
h (km)	V_P (km s^{-1})	V_S (km s^{-1})	ρ (g cm^{-3})	h (km)	V_P (km s^{-1})	V_S (km s^{-1})	ρ (g cm^{-3})	h (km)	V_P (km s^{-1})	V_S (km s^{-1})	ρ (g cm^{-3})	h (km)	V_P (km s^{-1})	V_S (km s^{-1})	ρ (g cm^{-3})
19	6.14	3.55	2.74	25	5.58	3.18	2.66	20	6.14	3.55	2.74	5	1.50	0.00	1.00
19	6.58	3.80	3.00	25	6.50	3.76	2.90	20	6.80	3.93	3.00	5	6.58	3.80	3.00
12	8.20	4.65	3.32	30	8.10	4.51	3.36	10	8.10	4.51	3.32	12	8.20	4.65	3.32
10	8.17	4.62	3.34	10	8.07	4.46	3.37	10	8.10	4.51	3.34	10	8.17	4.62	3.34
10	8.14	4.57	3.35	10	8.02	4.41	3.38	10	8.10	4.51	3.35	10	8.14	4.57	3.35
10	8.10	4.51	3.36	25	7.93	4.37	3.39	10	8.10	4.51	3.36	10	8.10	4.51	3.36
10	8.07	4.46	3.37	25	7.85	4.35	3.41	10	8.07	4.46	3.37	10	8.07	4.46	3.37
10	8.02	4.41	3.38	25	7.89	4.36	3.43	10	8.02	4.41	3.38	10	8.02	4.41	3.38
25	7.93	4.37	3.39	25	7.98	4.38	3.46	25	7.93	4.37	3.39	25	7.93	4.37	3.39
25	7.85	4.35	3.41	25	8.10	4.42	3.48	25	7.85	4.35	3.41	53	7.60	4.20	3.41
25	7.89	4.36	3.43	25	8.21	4.46	3.50	25	7.89	4.36	3.43	25	7.89	4.36	3.43
25	7.98	4.38	3.46	50	8.38	4.54	3.53	25	7.98	4.38	3.46	25	7.98	4.38	3.46
25	8.10	4.42	3.48	50	8.62	4.68	3.58	25	8.10	4.42	3.48	25	8.10	4.42	3.48
25	8.21	4.46	3.50	50	8.87	4.85	3.62	25	8.21	4.46	3.50	25	8.21	4.46	3.50
50	8.38	4.54	3.53	50	9.15	5.04	3.69	50	8.38	4.54	3.53	50	8.38	4.54	3.53
50	8.62	4.68	3.58	50	9.45	5.21	3.82	50	8.62	4.68	3.58	50	8.62	4.68	3.58
50	8.87	4.85	3.62	100	9.88	5.45	3.90	50	8.87	4.85	3.62	50	8.87	4.85	3.62
50	9.15	5.04	3.69		10.17	5.52	3.98	50	9.15	5.04	3.69	50	9.15	5.04	3.69
50	9.45	5.21	3.82					50	9.45	5.21	3.82	50	9.45	5.21	3.82
100	9.88	5.45	3.90					100	9.88	5.45	3.90	100	9.88	5.45	3.90
	10.17	5.52	3.98						10.17	5.52	3.98		10.17	5.52	3.98

* Continental model
† From Model 2 in Gomez *et al.* (1997a); 50 km thick crust
§ From Model 3 in Gomez *et al.* (1997a); 40 km thick crust
¶ Oceanic model

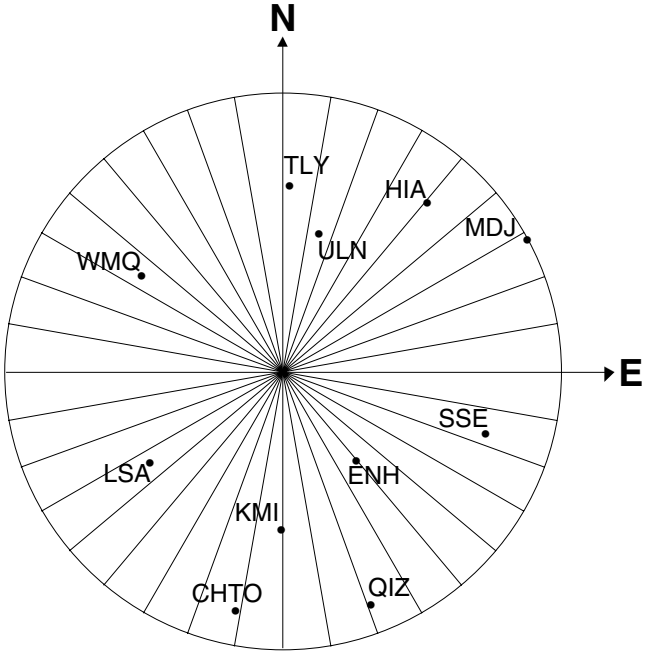

Figure 3. Azimuthal distribution of broad-band seismic stations selected for surface wave analysis of the Tianzhu (1996 June 1, $M_w = 5.2$) earthquake. Centre is epicentre location. Distance from centre is epicentral distance, maximum (21.5°) at MDJ.

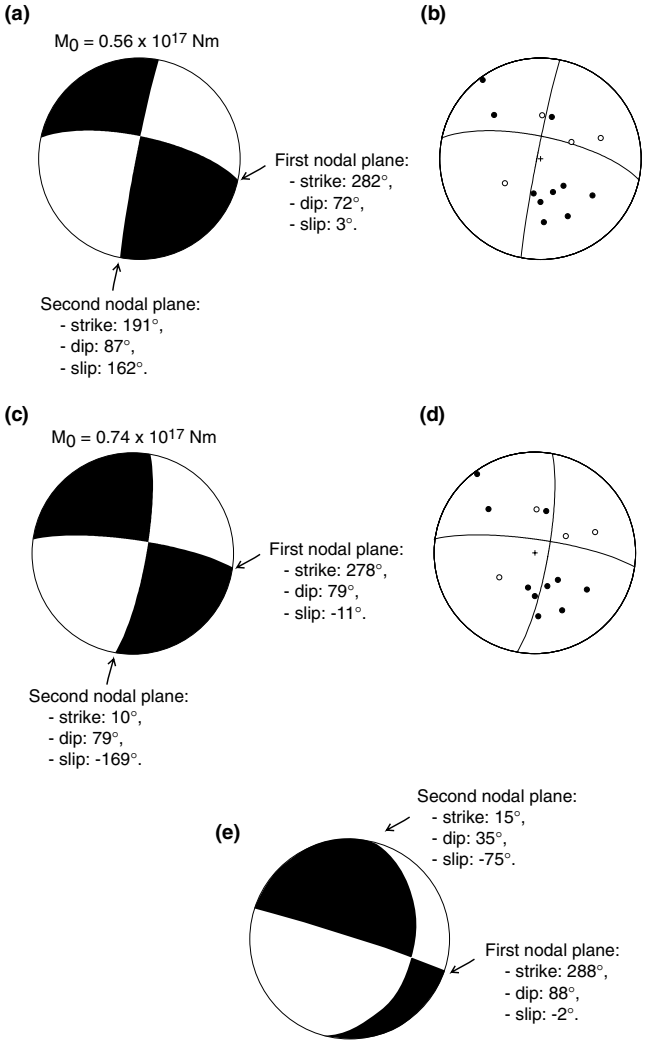

Figure 4. Tianzhu earthquake. (a) Moment tensor solution from joint inversion of surface waves amplitude spectra and polarities of *P*-wave first motions, superimposed in (b) on selected (see text) *P*-wave first-motion polarities from IRIS, GEOSCOPE and Chinese regional stations. (c) Moment tensor solution from Harvard, superimposed in (d) on *P* polarities. (e) Solution from SIL.

that estimated by Harvard (0.74×10^{17} N m). To give an idea of the resolution of the **P** (or **T**) orientation estimates, values of the partial residual function $\varepsilon_{\mathbf{P}}(\mathbf{P})$ [or $\varepsilon_{\mathbf{T}}(\mathbf{T})$] are plotted as a function of all possible orientations of the **P** compression (or **T** tension) axis (Fig. 5, lower-hemisphere stereographic projection). We also compare radiation patterns of the observed and synthetic amplitude spectra of Love and Rayleigh fundamental modes, normalized to a unique source–receiver distance of 2000 km and a horizontally homogeneous propagating medium similar to the source medium (Fig. 6 shows an example for a period of 27 s). Finally, the double-couple depth minimizing the partial residual function $\varepsilon_h(h)$ is around 12 km (Fig. 7). The depths estimated by Harvard, USGS and SIL are 15, 10 and 5 km, respectively.

3.1.2 *Tectonic interpretation*

According to SIL, the main shock of the Tianzhu earthquake was located $\simeq 6$ km west of the 10 km wide Tianzhu half-pull-apart basin and $\simeq 4$ km north of the Leng Long Ling segment of the Haiyuan fault (LLL in Figs 1 and 8a), which extends westwards from the southwestern tip of the basin. This segment is mainly strike-slip but fieldwork shows clear evidence of a normal throw component on the SSW-dipping fault plane (Gaudemer *et al.* 1995). Given this dip, as well as the SE dip of the normal fault in the pull-apart basin, and assuming that the uncertainty on SIL's epicentre location is less than 4 km, we can first conclude that the earthquake did not occur on the Haiyuan fault itself, and neither did it occur on the Gulang fault system, as could be preliminarily inferred from the Harvard centroid location of the main shock (Fig. 8a). To verify this conclusion and pursue the interpretation further, we studied part of the aftershocks of the Tianzhu event, recorded by a local network of six seismic stations (three-component, broad-band) that we installed on 1996 July 15, 1.5 months after the main shock. These aftershocks were located using the HYPO71 software (Lee & Lahr 1975). The method used to assess location uncertainties is inspired by that described in Jacques *et al.* (1999) and briefly summarized in Appendix B. We note that the aftershocks are located in the same area as the SIL main-shock epicentre, which seems to validate the SIL location and confirms that the main Haiyuan fault did not rupture during the Tianzhu event (Fig. 8a). The aftershock depths range between 10 and 16 km. Plotting hypocentres on vertical cross-sections perpendicular to the nodal planes of the main event does not reveal any clear structure. However, aftershocks do not necessarily activate a unique fault plane identical to that of the main shock; they can simply result from distributed deformation.

In the absence of a clear pattern in vertical section, we are thus left with two plausible scenarios to explain the Tianzhu rupture. The Maomao Shan segment of the Haiyuan fault (MMS, Figs 1 and 8a), northeast of the Tianzhu basin,

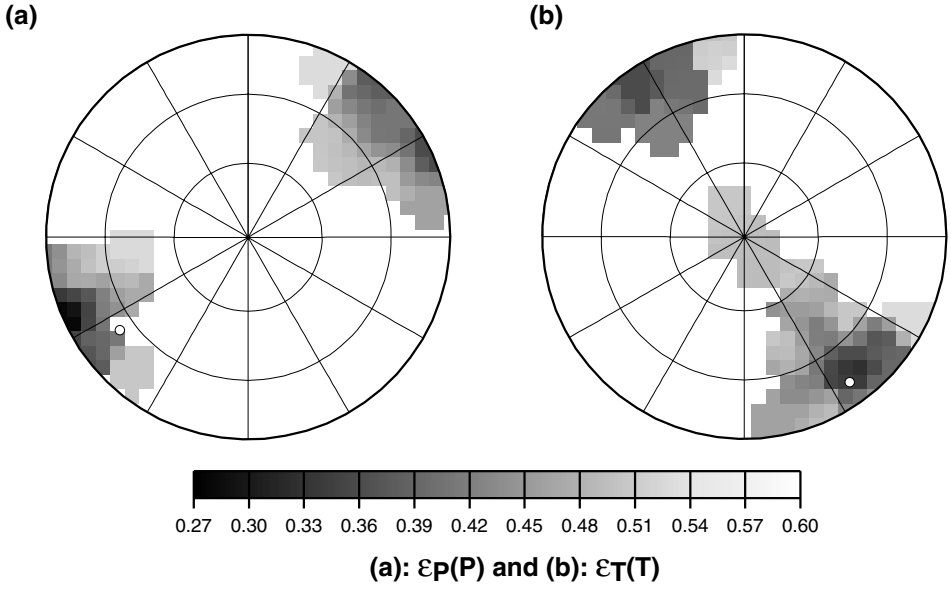

Figure 5. Tianzhu earthquake. Partial residual functions (a) $\varepsilon_{\mathbf{P}}(\mathbf{P})$ as a function of **P** compression axis orientation and (b) $\varepsilon_{\mathbf{T}}(\mathbf{T})$ as a function of **T** tension axis orientation. Each point is a stereographic projection of **P** (or **T**) on the lower hemisphere. White dots indicate, for comparison, the orientation of the corresponding principal stress axis of the Harvard focal mechanism.

continues westwards for 10–15 km, past the junction with the west Tianzhu normal fault. This 10 km long splay limits the aftershock area to the north and its trend is consistent, within 10°–15°, with the N101°E-striking nodal plane of our moment tensor solution. In the first scenario, the rupture could thus have been initiated on this splay, while the main Haiyuan fault would still be locked (model 1, Fig. 8b). Given the SIL location of the main event, this hypothesis would require a SSW-dipping fault plane of about 70°, in apparent disagreement with the corresponding NNE 72° dip predicted by our mechanism. However, a SSW 70°-dipping fault plane would remain in agreement with the observed polarities (Fig. 4b) and the associated **P**-axis would still correspond to a small value of $\varepsilon_{\mathbf{P}}(\mathbf{P})$ (<0.4, compared with the 0.28 minimum value, Fig. 5a). In the absence of relocation of the main shock, an epicentre location 3 km further north, within the error bars of this location, remains plausible, implying a nearly vertical fault plane, again not in disagreement with the polarities and giving a minimum value of $\varepsilon_{\mathbf{P}}(\mathbf{P})$ (Figs 4b and 5a).

The second scenario involves a dextral cross-fault, striking $\simeq$N25°E orthogonal to the fault plane considered above (model 2, Fig. 8b), compatible within 15° with the other N12°E-striking nodal plane of the calculated focal mechanism. No surface trace attests to the existence of such a dextral cross-fault, but given the magnitude and associated coseismic displacement (of the order of a few centimetres) of the event, a hidden fault at depth remains a possible candidate. The mechanism involved here would be book-shelf faulting, compatible with the main stress directions, during the interseismic period when the main Haiyuan fault is locked, and counterclockwise

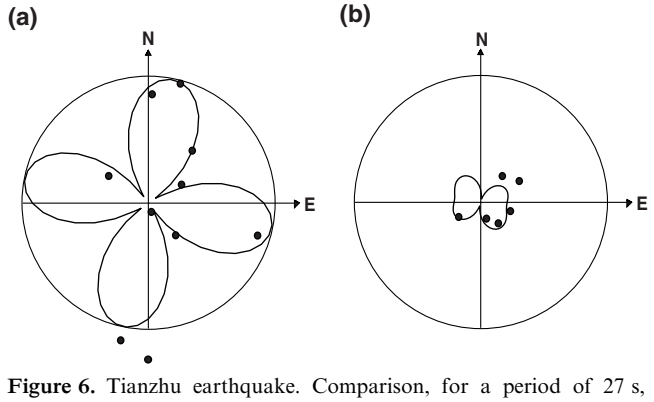

Figure 6. Tianzhu earthquake. Comparison, for a period of 27 s, of radiation patterns of observed (dots) and synthetic (solid line) amplitude spectra of (a) Love and (b) Rayleigh fundamental modes. Amplitudes are recalculated for a source–receiver distance of 2000 km and a laterally homogeneous velocity model, similar to the source region model. Circle radius is 0.02 cm s.

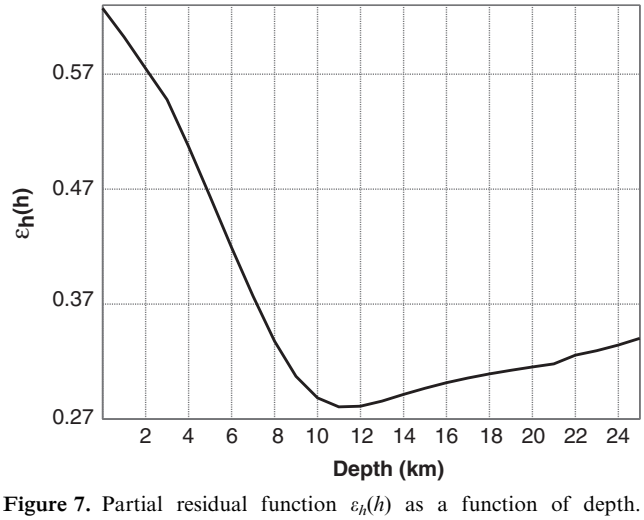

Figure 7. Partial residual function $\varepsilon_h(h)$ as a function of depth. Minimum is for a depth around 12 km.

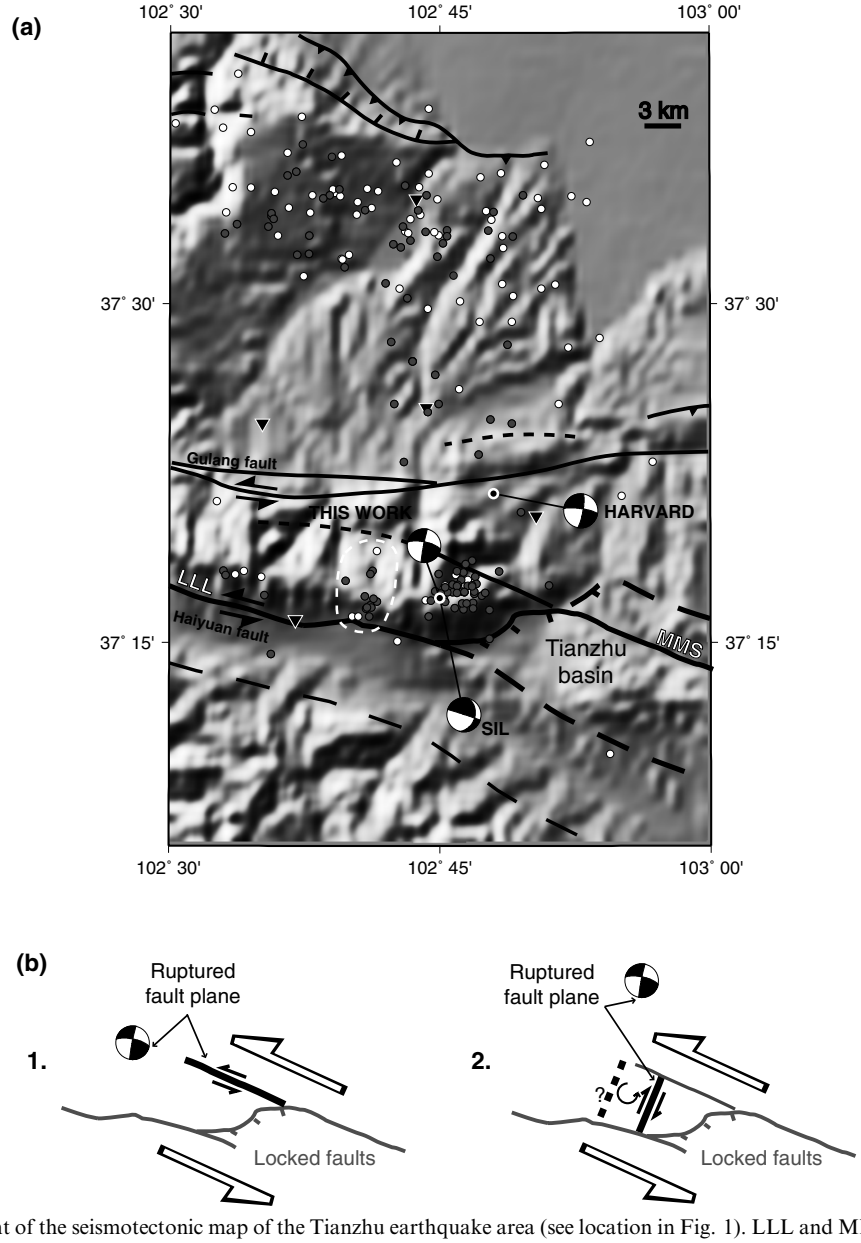

Figure 8. (a) Enlargement of the seismotectonic map of the Tianzhu earthquake area (see location in Fig. 1). LLL and MMS indicate the Leng Long Ling and Maomao Shan segments of the Haiyuan fault, respectively, separated by the Tianzhu half-pull-apart basin. Microseismicity was recorded by a local IPGP network of six three-component stations (five shown on map by triangles; see also Fig. 1) from July 1996 to July 1998. There are at least seven *P* and *S* arrival time readings. Estimated uncertainty on epicentre location is 2 km (grey dots) or 5 km (white dots). See Appendix B for details. The seismic swarm of March 1998 is encircled with a dashed white line. (b) Two plausible interpretations of rupture (see discussion in text).

block rotation might be favoured. The geometry and scenario of model 2 in Fig. 8(b) are reminiscent of the fault geometry and earthquake history observed southeast of the Salton Sea along the San Andreas fault system in southern California. Several parallel sinistral cross-faults, striking NE, limit the southeastern border of the right-stepping Salton Sea pull-apart. Such cross-faults are perpendicular to the dextral Imperial, Superstition Hills and Coyote Creek faults, south and southeast of the Salton Sea, and to the San Andreas fault, north and northwest of the Salton Sea. They partly connect the two dextral fault systems (Fig. 1 in Hudnut & Sieh 1989). Several earthquakes have ruptured these cross-faults, in 1979 (Johnson & Hutton 1982) and 1981 (Nicholson *et al.* 1986) and on the Elmore Ranch fault (1987 November 24, $M_s = 6.2$, a foreshock of the $M_s = 6.6$ event on the Superstition Hills fault; Hudnut *et al.* 1989). Regardless of the sense of horizontal slip (which is opposite on the San Andreas fault), we thus propose that the Tianzhu pull-apart, the dextral cross-fault involved in our second scenario and the Haiyuan fault system might be comparable to the Salton Sea pull-apart, the Elmore Ranch fault and the Superstition Hills San Andreas fault system. The aftershocks located may accommodate induced block deformation and contribute to releasing part of the stress (the cross-fault would limit the aftershocks to the west). Further west, a seismic swarm that occurred in March 1998 (Fig. 8a) might have activated a second, $\simeq$N25°E-striking fracture plane, thus delimiting a second block, in a final process of stress release (model 2, Fig. 8b).

3.2 Yongden earthquake

3.2.1 Results of inversion

We selected 16 stations to determine the source parameters of the Yongden earthquake (Fig. 9) and inverted amplitude spectra of Love and Rayleigh fundamental modes, at 10 and 11 stations (Table 4), respectively, for periods between 35 and 70 s. We fixed the latitude of the epicentre at 36.367°, its longitude at 103.25° and its origin time at 22:44:4.4 UT (data from SIL). The velocity model around the source is the same as for the Tianzhu earthquake (Table 2). Under the receivers (Table 4), models belong to the four classes defined in Table 3. *P* polarities are those read at IRIS and GEOSCOPE stations. We obtain a thrust focal mechanism with a first nodal plane of strike, dip and slip 105°, 45° and 75°, respectively, and a second nodal plane of strike, dip and slip 306°, 47° and 104°, respectively, again in good agreement with the Harvard CMT mechanism (Fig. 10). However, we find a more WNW–ESE orientation for the second nodal plane and a small strike-slip component. This slight difference remains within the limits of resolution of the method. Again, *P*-wave polarities seem to agree better with our solution than with the Harvard mechanism (Fig. 10). Seismic moments of the two solutions compare very well (this study: 2.4×10^{17} N m; Harvard: 2.7×10^{17} N m). The partial residual functions $\varepsilon_{\mathbf{P}}(\mathbf{P})$ and $\varepsilon_{\mathbf{T}}(\mathbf{T})$ are shown in Fig. 11. Observed and synthetic amplitude spectra of Love and Rayleigh radiation patterns, normalized to a source–receiver distance of 5000 km, are shown in Fig. 12. As signals at some stations could not be used in the whole period interval [35 s, 70 s], examples are given for two periods (40 and 64 s) sampling the whole set of stations used for each wave type. The best estimate for the double-couple depth is around 6 km (Fig. 13), shallower than the Harvard (15 km), USGS (12 km) and SIL (8 km) estimates.

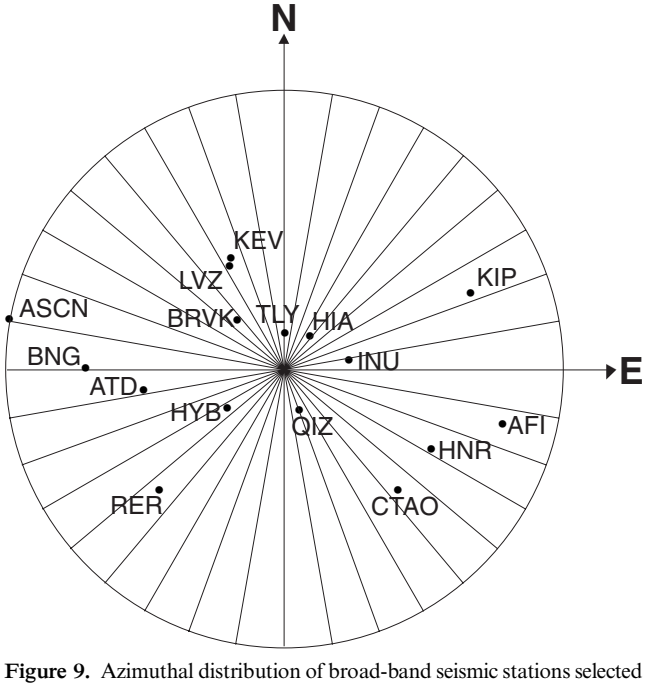

Figure 9. Azimuthal distribution of broad-band seismic stations selected for surface wave analysis of the Yongden (1995 July 21, $M_w = 5.6$) earthquake. Centre is epicentre location. Distance from centre is epicentral distance, maximum (117°) at ASCN.

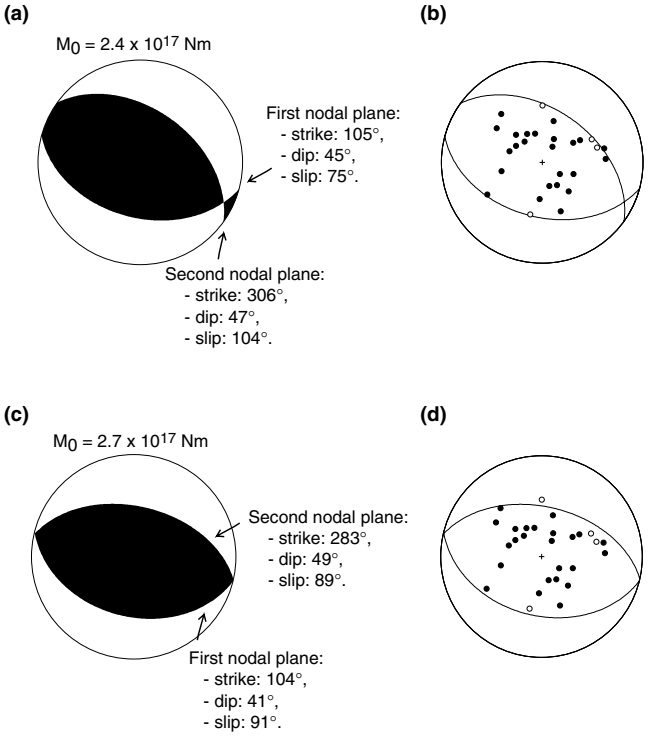

Figure 10. Yongden earthquake. (a) Moment tensor solution from joint inversion of surface wave amplitude spectra and polarities of *P*-wave first motions, superimposed in (b) on selected *P*-wave first-motion polarities (from IRIS and GEOSCOPE stations). (c) Moment tensor solution from Harvard, superimposed in (d) on *P* polarities at worldwide stations.

3.2.2 Tectonic interpretation

The Yongden epicentre location was, at first sight, puzzling. None of the active faults mapped thus far in the area could be convincingly associated with the earthquake. However, a detailed analysis of Landsat images and of the 30 arc s Defense Mapping Agency DEM reveals the existence, close to the epicentre, of uplifted surfaces mapped as Quaternary alluvial terraces (Gansu Geological Bureau 1975), tilted towards the southwest and roughly aligned in a N100°E direction (Figs 1 and 14). This direction is that of the first nodal plane of our Yongden focal mechanism (Fig. 10). West of the westernmost uplifted fan, upstream from Minhe, the Datong He becomes entrenched in a narrow gorge. We infer that this reflects incision by the Datong He in response to tectonic uplift, as do other gorges observed along the Huang He west and southwest of Lanzhou, where it crosses a succession of fast-rising mountain ranges (Van der Woerd 1998; Métivier *et al.* 1998; Meyer *et al.* 1998). West of the Datong gorge, Precambrian basement crops out (Fig. 14a). North of the uplifted Quaternary terraces, perpendicular to the Datong valley, extant geological maps show a $\simeq$N100°E-striking contact between Neogene and Cretaceous red beds (e.g. Gansu Geological Bureau 1975). The location, direction and extent of this contact, which crosses the Datong valley where it broadens upstream from the Minhe gorge, suggest that it might correspond to an active, SSW-dipping thrust bringing Cretaceous on top of Neogene. This contact would thus be mostly tectonic rather than stratigraphic. Such a thrust might have ruptured during the Yongden event and cumulative movement on it could be responsible for the

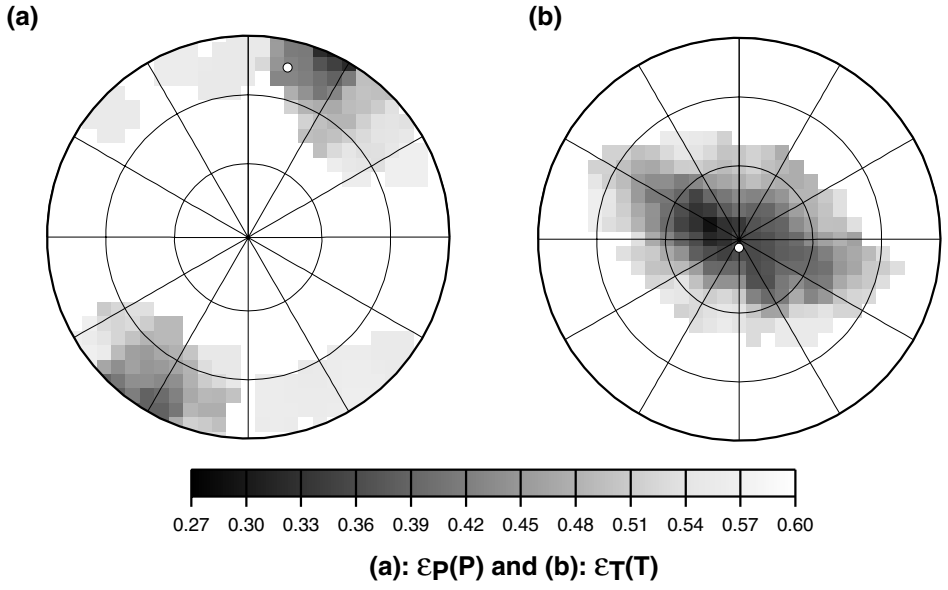

Figure 11. Yongden earthquake. Partial residual functions (a) $\varepsilon_{\mathbf{P}}(\mathbf{P})$ as a function of **P** compression axis orientation and (b) $\varepsilon_{\mathbf{T}}(\mathbf{T})$ as a function of **T** tension axis orientation on lower-hemisphere stereographic projections. White dots indicate, for comparison, the orientations of the corresponding principal stress axes of the Harvard focal mechanism.

Table 4. Seismic stations, wave types and models used for the inversion of the Yongden earthquake.

Station	Wave type*	Model†
ATD	R	1
BNG	L	1
BRVK	R, L	1
CTAO	R, L	1
HIA	R	1
HYB	R, L	1
INU	L	1
KEV	R	1
LVZ	L	1
QIZ	L	1
TLY	R, L	3
ASCN	L	4
AFI	R	4
HNR	R, L	4
KIP	R	4
RER	R	4

* R: Rayleigh; L: Love
† See Table 3

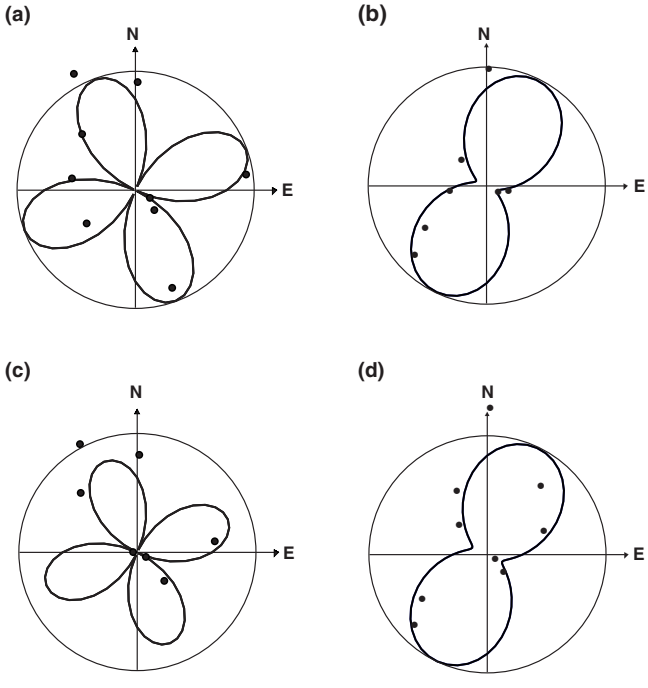

Figure 12. Yongden earthquake. Comparison, for a period of 40 s, of radiation patterns of observed (dots) and synthetic (solid line) amplitude spectra of (a) Love and (b) Rayleigh fundamental modes and comparison for a period of 64 s for (c) Love and (d) Rayleigh waves. Amplitudes are recalculated for a source–receiver distance of 5000 km and a laterally homogeneous velocity model, similar to the source region model. Maximum amplitudes are 0.024 cm s at 40 s and 0.017 cm s at 64 s.

observed local uplift, including that of the Precambrian basement (Fig. 14a). Mapping of the aftershocks of the earthquake, recorded at Chinese regional stations and compiled by the SIL, supports this interpretation (Fig. 14b). We thus infer that the N105°E nodal plane of Fig. 10 corresponds to the fault plane ruptured by the Yongden event.

Southeast of Lanzhou, a comparable SW-dipping thrust is mapped (e.g. Tapponnier & Molnar 1977). It may branch at depth off the NNW–SSE left-lateral strike-slip fault south of it (Fig. 1). We infer that this strike-slip fault continues northwestwards along the Huang Shui river, reaching a total length of $\simeq$150 km, and that the thrust associated with the Yongden earthquake also branches off it at depth (Fig. 14c). The surface traces of the faults, the earthquake's depth and the dip of the nodal plane we calculated are in overall agreement with this interpretation. Most of the aftershocks (2/3) projected on the N15°E cross-section of Fig. 14(c) plot near or above the thrust plane, which seems to be consistent with the inferred structure

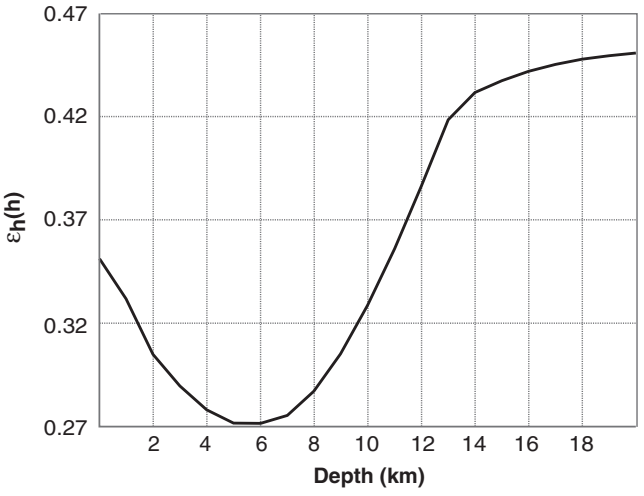

Figure 13. Partial residual function $\varepsilon_h(h)$ as a function of depth. The minimum is for a depth around 6 km.

at depth. Some, however, are located as deep as 30 km. In any case, the nearest regional seismic station likely to have recorded these aftershocks being 35–40 km distant from the Yongden epicentre, the aftershock depths are too poorly constrained to help in either confirming or dismissing our interpretation.

4 DISCUSSION AND CONCLUSIONS

4.1 Source parameters

FTAN and joint inversion of surface wave amplitude spectra using intermediate periods and polarities of *P*-wave first motions prove remarkably efficient in calculating the focal mechanisms, seismic moments and depths of the Tianzhu and Yongden moderate-sized earthquakes ($M_w \simeq 5.5$, $M_s \simeq 5$). We selected two events for which Harvard CMT solutions had been calculated. The comparison between these CMT mechanisms and our mechanisms is good.

The influence of velocity models on the estimates of source parameters has been tested. We repeated the inversion using the PREM model, instead of regional models, for all the receivers. The results did not change significantly, as already observed in previous studies (Gomez *et al.* 1997a). In order to estimate the separate contributions of surface wave amplitude spectra and *P* polarities on the final solution, we performed the inversion using surface wave amplitude spectra only. For each event, among the four equivalent solutions obtained in that case (Mendiguren 1977), one did not differ significantly from the result of joint inversion of surface wave amplitude spectra and *P*-wave first-motion polarities. Its resolution, however, was much poorer than in the joint inversion. The azimuthal station coverage was very good for both studied earthquakes. Finally, the stability of our solutions in the case of a less favourable station distribution was tested. The inversion results did not change significantly by reducing by up to three the number of stations with good records of both Love and Rayleigh fundamental modes, as long as the stations covered an azimuthal range of at least 90°.

The method presented here thus shows encouraging results. It now has to be applied to a larger set of earthquakes to test its reliability in source parameter determinations of $M_w \simeq 5.5$ and possibly even smaller events.

4.2 Tectonic implications

This study sheds light on two interesting earthquakes in a major seismic gap area. The first one, the Tianzhu earthquake, is an off-fault event near a major fault step in the centre of the gap, the Tianzhu pull-apart basin. From the strike-slip mechanism we have calculated, the epicentre location from SIL, the locations of aftershocks recorded by a local network, which significantly differ from the Harvard centroid locations, and fieldwork, we propose two scenarios. They involve secondary structures NW of the pull-apart, in a slip transfer zone between two segments of the Haiyuan fault, which remains locked. Such secondary faults are commonly observed at the ends of pull-aparts and dilational jogs, although geometries vary widely (see Zachariasen & Sieh 1995 and references therein). The occurrence of the earthquake close to a left step along the fault is probably not a coincidence. Previous studies (most recently Kato *et al.* 1999) have shown that earthquakes can initiate where the fault trace has bends and jogs, particularly extensional ones, such as pull-apart steps. We note that two other earthquakes of $M_l = 5$ and $M_l = 5.3$ (the corresponding M_l for the Tianzhu event is 5.6) occurred in 1956 and 1984, respectively (Chen *et al.* 1991), the former event $\simeq 10$ km southeast of the 1996 epicentre, possibly on another structure, and the latter $\simeq 5$ km north of it, possibly also on a cross-fault (Fig. 1). Whether the Tianzhu event is due to a normal stress release in a large fault bend area with no further implications, or whether it implies, together with the 2000 event, that the Haiyuan fault, after the 1986 and 1990 events (Fig. 1), is already in the pre-seismic part of its seismic cycle (Gaudemer *et al.* 1995), preceding a future larger event, remains unclear.

We tentatively identify, for the first time, a N100–105°E south-dipping active thrust north of the Huang Shui river as the most likely source of the Yongden event, on the basis of the calculated thrust focal mechanism, evidence of local tectonic uplift and of a N100°E geological contact, and the epicentral locations of the aftershocks recorded by the Chinese regional network. This thrust may be connected at depth with the strike-slip fault that runs south and west of Lanzhou over a total length of perhaps 150 km, in part following the Huang Shui river. Although further field evidence of Holocene movement on both faults is needed, attention should be paid to this secondary thrust–strike-slip fault system. While it cannot be compared, in terms of size and rate, to the Haiyuan fault system, it is much closer to Lanzhou, one of the largest cities of central China. A major historical event ($M \simeq 7.2$) is reported in 1125 AD near Lanzhou (Gu *et al.* 1989). This study suggests that the fault system we have identified could be associated with this 1125 AD event. At a larger scale, the 1927 $M \simeq 8$ earthquake (Fig. 1) probably activated a similar system. It probably occurred on a décollement, linking at depth the sinistral Haiyuan fault and the south-dipping thrusts bounding the north flank of the Qilian Shan (Gaudemer *et al.* 1995). At an even greater scale, the whole Qilian Shan thrust system branches off the strike-slip Kunlun fault at depth, through a décollement, before rooting into a south-dipping subduction zone (Meyer *et al.* 1998). Such thrust–strike-slip systems thus appear to be typical of the tectonics of northeastern Tibet at all scales. The relationship between the Haiyuan and Lanzhou

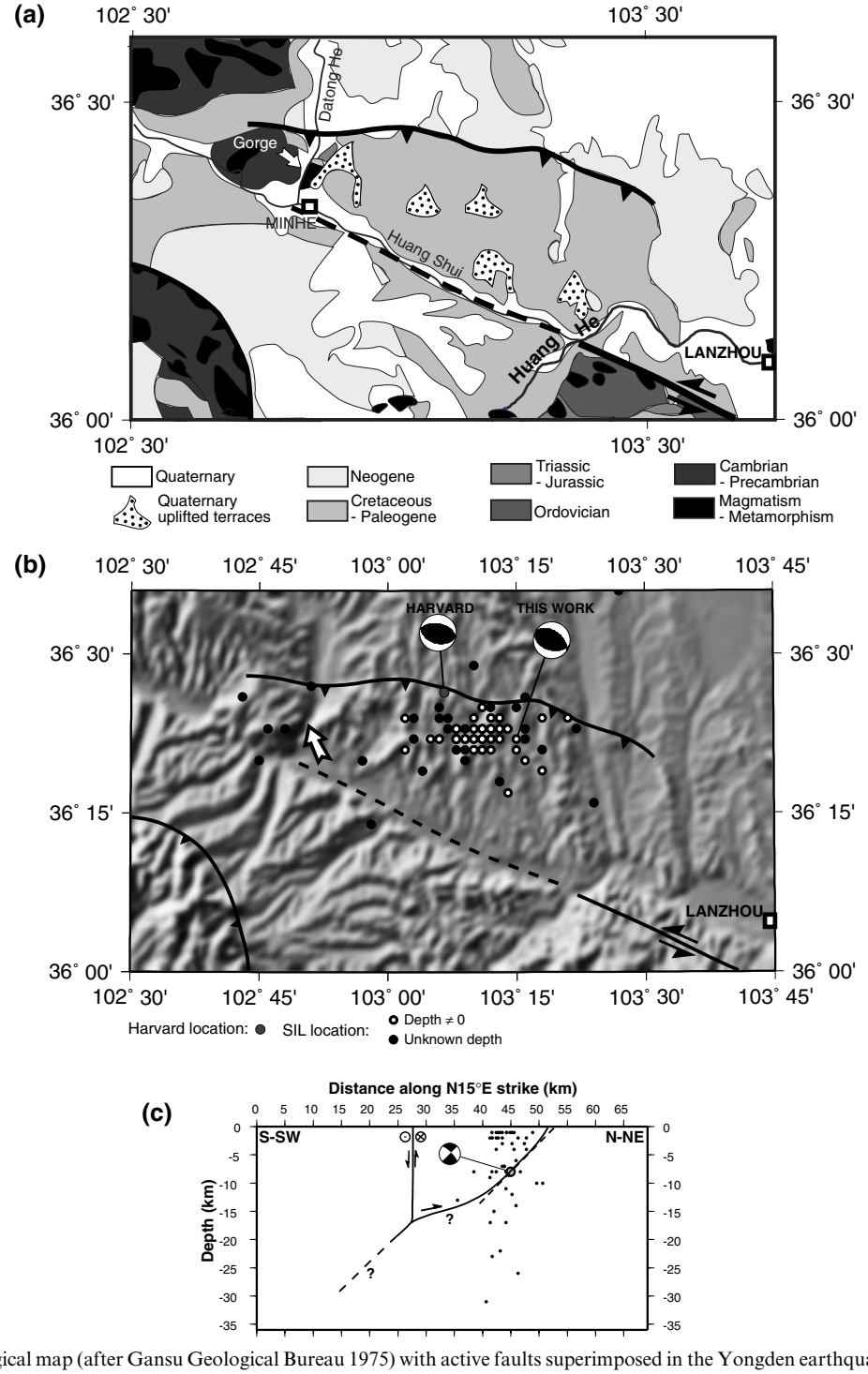

Figure 14. (a) Geological map (after Gansu Geological Bureau 1975) with active faults superimposed in the Yongden earthquake area (see location in Fig. 1). (b) Seismotectonic map of the same area. Black and white dots are aftershocks of the Yongden event located by SIL. Grey dot shows Harvard main shock location. White arrow points to narrow gorge (see text). Topography is from 30 arc s Defense Mapping Agency DEM. (c) Projection of aftershocks on N15°E-striking vertical plane, perpendicular to first nodal plane of our focal mechanism [point (0,0) is at latitude 36°N, longitude 103°E]. View, in vertical section, of proposed model for rupture at depth, compatible with fault surface traces, our moment tensor solution and slip partitioning between coupled strike-slip and thrust faults. For consistency with aftershock depths, the main shock is plotted at the SIL depth of 8 km.

fault systems, 100 km apart, needs further investigation. One may wonder whether triggering of the Yongden event might result from Coulomb stress increase due to the 20th century's major earthquakes along the Haiyuan fault, and what this might imply regarding the present seismic hazard near the Tianzhu seismic gap.

ACKNOWLEDGMENTS

This research was supported by the Institut Universitaire de France while BB and AM were visiting the Institut de Physique du Globe de Paris. We thank the Institut National des Sciences de l'Univers, Centre National de la Recherche Scientifique

(Programme PNRN) and the IPGP (programme BQR) for supporting monitoring and sustained work along the western Haiyuan fault. BB and AM were also supported by a subcontract with Cornell University, Geological Sciences, under EAR-9804858 from the US National Science Foundation, by the Russian Foundation of Fundamental Research, project 99-05-64964, the International Science and Technology Centre, project 1293-99 and INCO-COPERNICUS, contract ERBI-CI5CT960207. Reviews by T. Dahm and an anonymous reviewer helped considerably to clarify and improve the manuscript. We thank P. Ihmlé for having initiated this study and J. M. Gomez for helpful discussions. This is IPGP contribution 1707 and INSU contribution 241.

REFERENCES

Arvidsson, R. & Ekström, G., 1998. Global CMT analysis of moderate earthquakes, $M_w \geq 4.5$, using intermediate-period surface waves, *Bull. seism. Soc. Am.,* **88,** 1003–1013.

Babich, V., Chikachev, B. & Yanovskaya, T., 1976. Surface waves in a vertically inhomogeneous elastic half-space with weak horizontal inhomogeneity, *Izv. Akad. Nauk SSSR, Fisika Zemli,* **4,** 24–31.

Barka, A. & Kadinsky-Cade, K., 1988. Strike-slip fault geometry in Turkey and its influence on earthquake activity, *Tectonics,* **7,** 663–684.

Braunmiller, J., Dahm, T. & Bonjer, K.-P., 1994. Source mechanism of the 1992 Roermond earthquake from surface wave inversion of regional data, *Geophys. J. Int.,* **116,** 663–672.

Bukchin, B., 1989. Estimation of earthquake source parameters, in *Seismic surface waves in a laterally inhomogeneous earth*, pp. 229–245, ed. Keilis-Borok, V., Kluwer, Dordrecht.

Bukchin, B., 1990. Determination of source parameters from surface waves recording allowing for uncertainties in the properties of medium, *Izv. Akad. Nauk SSSR, Fizika Zemli,* **25,** 723–728.

Bukchin, B., 1995. Determination of stress glut moments of total degree 2 from teleseismic surface waves amplitude spectra, *Tectonophysics,* **248,** 185–191.

Bukchin, B., Levshin, A., Ratnikova, L., Dost, B. & Nolet, G., 1994. An estimate of spatial-temporal characteristics of the source for Spitak earthquake using broad-band records of surface waves, in *Computational Seismology and Geodynamics,* Vol. 2, pp. 156–161, ed. Chowdhery, D., AGU, Washington, DC.

Center for Analysis and Prediction, CSB, 1989. *Earthquake Catalogue in West China,* Science Press, Beijing.

Chen, J., Zhuang, C., Li, Q., Song, R., Xiu, J., Wu, N. & Chen, P., eds., 1991. *Summary Catalog of Chinese Earthquakes of Different Historical Periods (780 BC–1984 AD),* Seismological Press, Beijing.

Deng, Q., *et al.*, 1986. Variations in the geometry and amount of slip on the Haiyuan (Nanxihaushan) fault zone, China, and the surface rupture of the 1920 Haiyuan earthquake, in *Earthquake Source Mechanics, Geophys. Monogr. Ser.,* Vol. 37, pp. 169–182, eds Das, S., Boatwright, J. & Scholz, C., AGU, Washington, DC.

Dziewonski, A., Chou, T.-A. & Woodhouse, J., 1981. Determination of earthquake source parameters from waveform data for studies of global and regional seismicity, *J. geophys. Res.,* **86,** 2825–2852.

Ekström, G. & Richards, P., 1994. Empirical measurements of tectonic moment release in nuclear explosions from teleseismic surface waves and body waves, *Geophys. J. Int.,* **117,** 120–140.

Gansu Geological Bureau, 1975. *Geological map of Gansu, scale 1:1 000 000,* Geological Press, Beijing.

Gaudemer, Y., Tapponnier, P., Meyer, B., Peltzer, G., Guo, S., Chen, Z., Dai, H. & Cifuentes, I., 1995. Partitioning of crustal slip between linked active faults in the eastern Qilian Shan, and evidence for a major seismic gap, the 'Tianzhu gap', on the western Haiyuan fault, Gansu (China), *Geophys. J. Int.,* **120,** 599–645.

Given, J. & Mellman, J., 1986. Estimating explosions and tectonic source parameters of underground nuclear explosions from Rayleigh and Love wave observations, *Tech. Rept,* US Air Force Geophysical Laboratory, MA.

Gomez, J., 1998. Étude spatio-temporelle de la rupture, *PhD thesis,* Université Paris 7, France.

Gomez, J., Bukchin, B., Madariaga, R., Rogozhi, E. & Bogachkin, B., 1997a. Rupture process of the 19 August 1992 Susamyr, Kyrgyzstan, earthquake, *J. Seismol.,* **1,** 219–235.

Gomez, J.M., Bukchin, B., Madariaga, R. & Rogozhin, E.A., 1997b. A study of the Barisakho, Georgia earthquake of October 23, 1992 from broad band surface and body waves, *Geophys. J. Int.,* **129,** 613–623.

Gu, G., Lin, T. & Shi, Z., 1989. *Catalogue of Chinese Earthquakes (1831 BC–1969 AD),* Science Press, Beijing.

Hudnut, K.W. & Sieh, K.E., 1989. Behavior of the Superstition Hills fault during the past 330 years, *Bull. seism. Soc. Am.,* **79,** 304–329.

Hudnut, K.W., Seeber, L. & Pacheco, J., 1989. Cross-fault triggering in the November 1987 Superstition Hills earthquake sequence, southern California, *Geophys. Res. Lett.,* **16,** 199–202.

Jacques, E., Ruegg, J., Lépine, J., Tapponnier, P., King, G. & Omar, A., 1999. Relocation of $M \geq 2$ events of the 1989 Dôbi seismic sequence in Afar: evidence for earthquake migration, *Geophys. J. Int.,* **138,** 447–469.

Johnson, C.E. & Hutton, L.K., 1982. Aftershocks and pre-earthquake seismicity, in *The Imperial Valley Earthquake of October 15, 1979, USGS Prof. Paper,* **1254,** 59–76.

Kato, N., Satoh, T., Lei, X., Yamamoto, K. & Hirasawa, T., 1999. Effect of fault bend on the rupture propagation process of stick-slip, *Tectonophysics,* **310,** 81–99.

King, G. & Nabelek, J., 1985. Role of fault bends in the initiation and termination of earthquake rupture, *Science,* **228,** 984–987.

Lander, A., 1989a. Frequency-time analysis, in *Seismic Surface Waves in a Laterally Inhomogeneous Earth*, pp. 153–163, ed. Keilis-Borok, V., Kluwer, Dordrecht.

Lander, A., 1989b. Linear polarization analysis, in *Seismic Surface Waves in a Laterally Inhomogeneous Earth,* pp. 164–178, , ed. Keilis-Borok, V., Kluwer, Dordrecht.

Lasserre, C., *et al.*, 1999. Postglacial left slip-rate and past occurrence of $M \geq 8$ earthquakes on the western Haiyuan fault, Gansu, China, *J. geophys. Res.,* **104,** 17 633–17 651.

Lee, W. & Lahr, J., 1975. HYPO71 (revised): a computer program for determining hypocenter, magnitude, and first motion pattern of local earthquakes, *USGS Open-File Rept,* Menlo Park, CA.

Levshin, A., 1985. Effects of lateral inhomogeneity on surface wave amplitude measurements, *Ann. Geophys.,* **3,** 511–518.

Levshin, A., Ritzwoller, M. & Ratnikova, L., 1994. The nature and cause of polarization anomalies of surface waves crossing northern and central Eurasia, *Geophys. J. Int.,* **117,** 577–591.

Ma, X., 1987. *Lithospheric Map of China,* Geological Publishing House, Beijing.

Mendiguren, J., 1977. Inversion of surface wave data in source mechanism studies, *J. geophys. Res.,* **82,** 889–894.

Métivier, F., Gaudemer, Y., Tapponnier, P. & Meyer, B., 1998. Northeastward growth of the Tibet plateau deduced from balanced reconstruction of two depositional areas: the Qaidam and Hexi corridor basins, China, *Tectonics,* **17,** 823–842.

Meyer, B., Tapponnier, P., Bourjot, L., Métivier, F., Gaudemer, Y., Peltzer, G., Guo, S. & Chen, Z., 1998. Crustal thickening in Gansu-Qinghai, lithospheric mantle subduction, and oblique, strike-slip controlled growth of the Tibet Plateau, *Geophys. J. Int.,* **135,** 1–47.

Nicholson, C., Seeber, L., Williams, P. & Sykes, L., 1986. Seismic evidence for conjugate slip and block rotation within the San Andreas fault system, southern California, *Tectonics,* **5,** 629–648.

Nielsen, S. & Knopoff, L., 1998. The equivalent strength of geometrical barriers to earthquakes, *J. geophys. Res.,* **103,** 9953–9965.

Tapponnier, P. & Molnar, P., 1977. Active faulting and tectonics in China, *J. geophys. Res.,* **82,** 2905–2930.

Van der Woerd, J., 1998. Couplage cinématique entre décrochements et chevauchements actifs dans le nord du Tibet. Croissance du plateau tibétain, *PhD thesis,* Université Paris 7, France.

Woodhouse, J., 1974. Surface waves in the laterally varying structure, *Geophys. J. R. astr. Soc.,* **90,** 12 713–12 728.

Zachariasen, J. & Sieh, K., 1995. The transfer of slip between two en echelon strike-slip faults: a case study from the 1992 Landers earthquake, southern California, *J. geophys. Res.,* **100,** 15 281–15 301.

Zhang, P., *et al.*, 1988. Bounds on the Holocene slip rate of the Haiyuan fault, north-central China, *Quat. Res.,* **30,** 151–164.

Zhang, P., *et al.*, 1988. Bounds on the average recurrence interval of major earthquakes along the Haiyuan fault in north-central China, *Seism. Res. Lett.,* **59,** 81–89.

Zhang, W., Jiao, D., Zhang, P., Molnar, P., Burchfiel, B.C., Deng, Q., Wang, Y. & Song, F., 1987. Displacement along the Haiyuan fault associated with the great 1920 Haiyuan, China, earthquake, *Bull. seism. Soc. Am.,* **77,** 117–131.

APPENDIX A: POLARITY SMOOTHING BEFORE INVERSION

We consider a set of n *P*-wave first-motion polarities (denoted $+1$ for compression and -1 for dilatation) observed at different seismic stations. We explore the space in all directions from the source, by sectors of small solid angle, and count the number of compression and dilatation polarities in each sector. If the number of polarities of one of the two classes is significantly larger than the number of opposite polarities, then the predominant polarity is attributed to the whole sector. If none of the two classes can be considered predominant (the decision criteria for this are detailed below), no polarity is used in the source parameter inversion for this sector. This procedure leads to smoothing of the initial polarity information.

We assume that, in each sector, polarities $+1$ and -1 appear randomly with the same probability, 1/2. If this hypothesis is true, then n_+, the number of observed positive polarities in the sector, and $n_- = n - n_+$, the number of negative ones, are random values distributed according to a binomial law, with mean $M(n_+)$ and $M(n_-)$, respectively, of $n/2$ and dispersion $D(n_+)$ and $D(n_-)$, respectively, of $n/4$. We define m as $m = n_+ - n_- = 2n_+ - n$, a random value, linear function of n_+, $M(m) = 2M(n_+) - n = n - n = 0$ as its mean, $D(m) = 4D(n_+) = n$ as its dispersion and $\sigma(m) = \sqrt{n}$ as its standard deviation.

One class of polarity is defined as predominant if $|m|$ is larger than its standard deviation. As a result,

(i) If $|m| \geq \sqrt{n}$ and $m > 0$, a polarity $+1$ is attributed to the whole sector,

(ii) if $|m| \geq \sqrt{n}$ and $m < 0$, a polarity -1 is attributed to the whole sector,

(iii) if $|m| < \sqrt{n}$, no polarities are used in the corresponding sector.

APPENDIX B: SELECTION AND UNCERTAINTY ON LOCATIONS OF TIANZHU EVENT AFTERSHOCKS

Three different velocity models were tested when running HYPO71 (Lee & Lahr 1975): a reference regional velocity model from SIL and the same model but with the *P* and *S* velocities of each layer increased by 5 per cent then decreased by 5 per cent. In the end, we only kept aftershocks with at least seven *P* or *S* traveltime readings available and call 'best epicentres' those whose epicentre locations remain stable within ± 2 km when changing the velocity structure, and for which the convergence criteria of HYPO71 are low (rms ≤ 0.25 s, *erh* and *erz* ≤ 2 km) and 'best hypocentres' those whose depths, in addition, remain stable within ± 2 km. 'Good epicentres' and 'good hypocentres' are defined as above, replacing 2 km by 5 km and 0.25 s rms by 0.4 s rms. Best and good epicentres are plotted in Fig. 8(a).